

Thermodynamics of aerosols during a molten core-concrete interaction at Fukushima Daiichi Unit 2 estimated conditions

Hugo LAFFOLLEY^{1,2}, Christophe JOURNEAU¹, Sarah THILLIEZ¹, Bernd GRAMBOW²

¹: CEA, DES, IRESNE, DTN, Severe Accident Experimental Laboratory, Cadarache F-13108 St-Paul-lez-Durance, France

²: SUBATECH (IMT Atlantique, CNRS-IN2P3, University of Nantes) 44307 Nantes, France

hugo.laffolley@cea.fr

ABSTRACT

Several radioactive releases from the containment took place during all the events leading up to Fukushima Daiichi endstate. Radionuclides released into the environment may differ in their composition or chemical form depending on the unit involved in the discharge and depending on the course of the accident. These differences may result from the path of the radionuclides from the core to the environment (e.g. through suppression pool water) and from the chemical and physical properties within the reactor core and the containment.

On March 14th and 15th 2011, spherical glassy Cs-bearing microparticles (type-A CsMP) were collected for the first time. These microparticles might result from molten core-concrete interaction (MCCI) inside Unit 2, where the Zircaloy from the fuel cladding interacted with the SiO₂ of the concrete pedestal at high temperature. The result of this interaction is a significant release of silica-rich gases or aerosols from the melt pool, which condense in colder locations.

Calculations using ThermoCalc with OECD/NEA's database TAF-ID version 11 were performed on the thermodynamics of vaporization during an MCCI to find correlations between the chemical and physical properties of the reactor atmosphere and the chemical composition of type-A CsMP. Data from ORIGEN2 and MELCOR calculations were used to estimate the core melt and atmosphere composition at the assumed time of the reactor pressure vessel failure.

The vapour temperature at which type-A CsMP may have condensed in the containment has been evaluated. Using Fe/Si, U/Si and Cs/Si ratios in the observed CsMP as an indicator for vapour composition, this suggests that type-A CsMP originate from condensation of vapours around 2000-2200°C from a low oxidised composition of corium, rich in zirconium and poor in stainless steel.

KEYWORDS

Molten core-concrete interaction, Aerosol, CsMP, TAF-ID

1. INTRODUCTION

In March 2011, 3 Units of the Fukushima Daiichi Nuclear Power Station (FDNPS) experienced severe accidents triggered by a magnitude 9.0 earthquake followed by a tsunami, causing a station black-out and loss of coolant to the reactor fuel. The reactor core's heat-up and degradation finally resulted in airborne

radioactive releases onto Japanese lands and into the Pacific Ocean [1]. Air dose rate monitoring and soil contamination surveys were carried out following the accident to investigate the magnitude of the releases. Cs^{134} and Cs^{137} (half-lives of 2.07 years and 30.08 years respectively [2]) are among the most volatile and abundant fission products of a reactor core [3]. It has been estimated that the total release of Cs^{137} caused by FDNPS ranges from 20.1 to 53.1 PBq [4]. Chemical forms and properties of radionuclides can vary depending on their source or their path from the molten fuel pellet into the atmosphere, and have a significant impact on their behaviour in the environment.

A research team located in Tsukuba city, Ibaraki prefecture (Japan), 170 km southwest of FDNPS, discovered a new kind of radioactive particles collected on an atmospheric filter [5]. The study reports Si-rich spherical particles with a diameter around 2 μm and containing radiocesium. Further analysis confirmed the amorphous SiO_2 matrix of these Cesium-bearing microparticles (CsMP) in addition to the presence of other major elements (Cs, K, Rb, Fe, Zn, Na, etc.) [6] and very recent work also reports a high content in C [7] or the presence of segregated phases of U [8]. Due to this silica matrix, CsMP have a very low solubility and a high stability in the environment [9] or in the respiratory system [10], [11]. Analyses of surface soil samples estimate that CsMP can account for 30% of the total Cs radioactivity in the trajectory of major plumes and even more than 40% of the total Cs radioactivity at some specific sampling sites [12].

Motivated by major environment and health concerns, research has been actively conducted on CsMP to assess their composition, solubility, abundance, etc. [6]. However, the physical phenomena leading to their formation are still fraught with many uncertainties that affect our understanding of the cesium phenomenology during the accident. With a view to improving the knowledge of their generation process, this article reports thermodynamic calculations using compositions and results from the OECD/NEA-Benchmark Study of the Accident at Fukushima Daiichi Nuclear Power Station (BSAF) project [13].

2. HYPOTHESIS AND DATA INPUT PARAMETERS

2.1. Database and Calculation Software

2.1.1. Database

The calculations are carried out using the Thermodynamics of Advanced Fuels – International Database (TAF-ID) version 11 developed by OECD/NEA. The TAF-ID was created using the CALPHAD method [14] and is designed for calculations on nuclear fuels. Fission products (FP) and structural materials are also considered to provide results under normal operation and accidental conditions of a reactor core [15]. A total of 43 elements are available in the TAF-ID.

For this study, the TAF-ID was chosen for its greater number of elements and particularly the availability of nitrogen and cesium, in addition to major elements related to severe accident studies.

2.1.2. Calculation software

The software chosen for the thermodynamic calculations is Thermo-Calc (versions 2017b and 2019a). Thermo-Calc is a calculation software based on the CALPHAD method that is compatible with the TAF-ID [15].

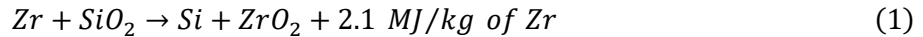
2.2. Hypothesis

2.2.1. Generation process

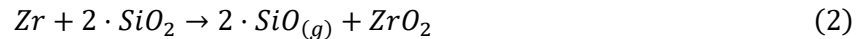
Knowledge about the generation process of CsMP is still unclear but several hypotheses have been put forward. The silica matrix implies that the generation process must include an abundant source of silicon. It could be stainless steel from the reactor pressure vessel (RPV) and from the structural materials [16],

insulating materials from the primary loop [17], atomisation of high-efficiency particulate air filters [18] or concrete from the pedestal after lower head failure (LHF) [9], [19], [20].

Molten core-concrete interaction (MCCI) is a likely source of silicon as Units 1 to 3 experienced lower head failure and experimental work showed that MCCI produces a significant amount of silica-rich aerosols that may have CsMP characteristics [21], [22]. When hot non-oxidised zirconium from the fuel rod cladding hits the concrete pedestal, a highly exothermic chemical reaction takes place [23].



This reaction occurs simultaneously with an incomplete reaction forming $\text{SiO}_{(g)}$ instead of Si as the temperature increases [24].



With a sufficient oxygen partial pressure, the oxidation of silicon can then be complete and form silica. Once gaseous silicon species are generated in a hot location, their migration by convection to a colder location of the primary containment vessel (PCV) causes condensation to form microparticles of amorphous silica through homogeneous or heterogeneous nucleation. At the same time, other volatile species such as Cs (possibly as CsOH) or Fe (possibly as an oxide) may be trapped inside the growing particles (Figure 1). The entrainment of droplets from bubble burst from the melt pool might be a source of aerosol during MCCI, but the composition of CsMP would be much more similar to the corium composition [22].

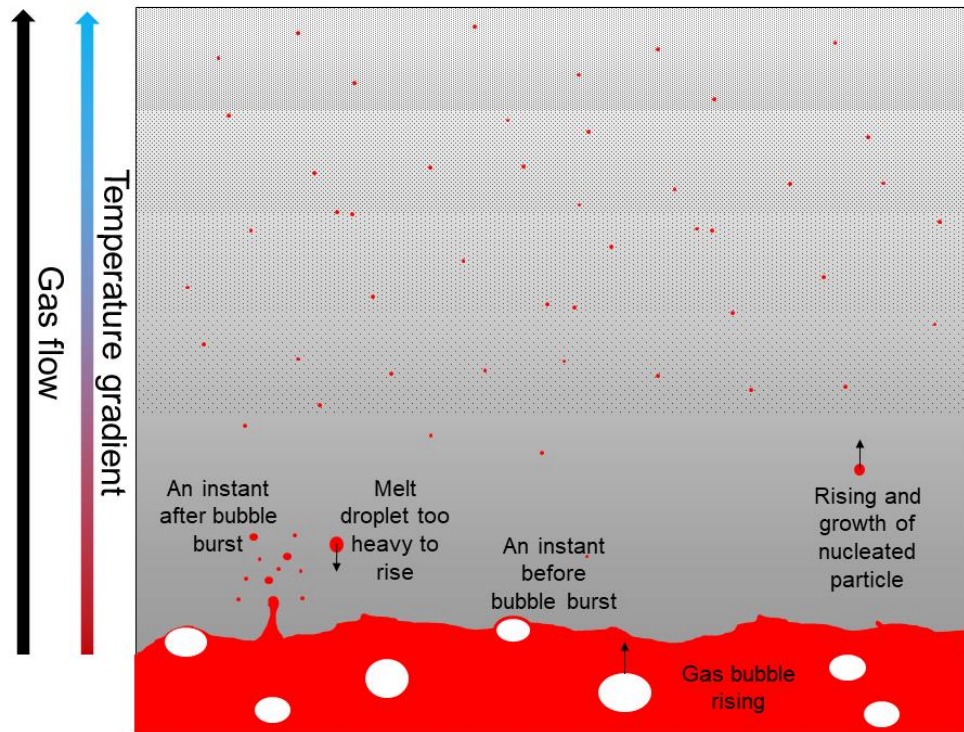


Figure 1. Possible generation mechanism of CsMP.

2.2.2. Unit of origin

During the FDNPS accident, units 1 (1F1), 2 (1F2) and 3 (1F3) underwent a loss of coolant in the primary loop, resulting in partial or complete meltdown of the reactor core [1]. Through the burnup ratio of each fuel

assembly, the ORIGEN2 code indicates the assembly specific and average amount of radionuclides in each reactor core and spent fuel pool [25]. Nuclear fuel of a reactor core is never entirely renewed with each reloading, but rather partly as well as relocated to optimise energy recovery from the fuel. Thus, radionuclides amount varies significantly depending on subassembly history. In the case of a partially melted core, it is therefore imprecise to infer the local amount of radionuclides from a global perspective. However, analytical results from the ORIGEN2 code show that on March 11, the average $^{134}\text{Cs}/^{137}\text{Cs}$ activity ratios for 1F1, 1F2 and 1F3 were 0.941, 1.08 and 1.05, respectively [25]. Therefore, the so-called type-A CsMP (i.e. those with a diameter below 10 μm and a high specific radioactivity [6]) have been associated with 1F2 or 1F3 as their $^{134}\text{Cs}/^{137}\text{Cs}$ activity ratio is generally higher than 1.0 even though heterogeneities exist in each of the three reactor cores. It is currently uncertain whether type-A CsMP are from 1F2, 1F3 or both. A TEPCO report yet refers to a glassy particle identifiable as a Type-A CsMP, found on the operating floor of the Unit 2 reactor building [26]. In this study, therefore, 1F2 is considered as the hypothetical unit of origin of CsMP for calculation.

2.2.3. Choice of elemental tracers

Quantitative or semi-quantitative chemical analyses of major species in CsMP have been reported in references [7], [27], [28]. The chemical composition of CsMP can be considered as an indicator of the chemical conditions prevailing in the reactor at the time they were formed. Thus, gas phase thermodynamic calculations could be used as a forensic tool to determine the chemical and physical conditions inside the reactor.

In the following work, Si, Fe, U, and Cs are used as chemical tracers to determine, through thermodynamic calculations, the temperature that provides a vapour composition consistent with actual CsMP composition. These major chemical elements of the reactor core and structure could also be selected based on their availability in the TAF-ID, their availability in the literature on CsMP chemical analysis and the ability to quantify the initial content of this element in the melt pool involved in the MCCI.

Table I was compiled from the chemical analysis carried out on 37 type-A CsMP [7]. This table provides the target range (between maximum and minimum) that vapour composition should achieve in order to match with the CsMP composition.

Table I. Minimum, median and maximum values of Fe/Si, U/Si and Cs/Si atomic ratios based on the chemical analysis of 37 CsMP [7].

Element	Minimum	Median (spherical)	Median (non-spherical)	Maximum
Fe/Si	0.10	0.23	0.19	0.33
U/Si	-	0.0015	0.0021	0.014
Cs/Si	0.019	0.069	0.077	0.23

2.3. Data Input Parameters

2.3.1. Reactive atmosphere composition and physical properties

In the first few years after the accident, it was unclear whether Unit 2 RPV experienced an LHF and whether the fuel had completely or partially relocated on the concrete pedestal [29]. Later, camera inspections of the Unit 2 PCV showed fuel debris on the concrete pedestal and confirmed the RPV failure [30]. There are still many uncertainties about the timing LHF occurred, some institutes of the BSAF project estimated that it happened between 83 and 129 hours after scram, but the first isolated CsMP were collected between 78 and 90 hours after scram.

In normal operation, PCV are filled with nitrogen at atmospheric pressure to prevent explosion in case of hydrogen build-up. However, during core degradation, Unit 2 PCV experienced pressure rise due to venting

and eventually leak from the RPV. Measurements show that the PCV pressure varied between 1 bar(a) and 7 bar(a) from scram to the RPV failure. Gas vented from the RPV to the PCV are initially only composed of water vapour but can progressively contain hydrogen from Zircaloy oxidation and gaseous fission products after cladding failure. MELCOR code calculations have been performed by Sandia National Laboratories* teams to study the progression of the accident in Unit 2 and LHF has been estimated to occur at about 91.5 hours after scram. These calculations suggest that the composition of the atmosphere in the PCV was mostly water vapour during this period and less than 1% of nitrogen and hydrogen.

However, the exact LHF time and the proportion of nitrogen, hydrogen and water vapour in the atmosphere are uncertain and the PCV atmosphere has to be estimated to perform the following thermodynamic calculations. Hence, the sensitivity analysis evaluates the influence of the atmosphere composition on the gas phase composition (3.1).

2.3.2. Corium composition

A large amount of Si and Zr should be available for the assumed chemical reactions (1) and (2), and the corium is highly unlikely to be fully oxidised when hitting the concrete. Table II and Table III list in-vessel and ex-vessel compositions from the BSAF project (1F2). The KAERI composition is not used as it consists only of stainless steel and its oxides [13].

2.3.3. Concrete composition

The concrete used for the FDNPS building is a basaltic concrete. Its composition has been estimated from the analysis of samples collected on 1F1 reactor building : $\text{SiO}_2 = 59.6\%$ wt., $\text{Al}_2\text{O}_3 = 14.7\%$, $\text{CaO} = 12.2\%$, $\text{H}_2\text{O} = 7.8\%$ et $\text{Fe}_2\text{O}_3 = 5.7\%$ [31].

Table II. Unit 2 in-vessel corium composition (data from chart [13]).

Species (%.wt)	Institutes					Average	
	CIEMAT	CRIEPI	IAE	IBRAE	KAERI	All institutes (Ci1)	Except IBRAE & KAERI (Ci2)
UO_2	55	30	16	49	0	30	34
Zr	29	52	16	51	0	30	32
ZrO_2	10	6	45	0	0	12	20
SS^\dagger	5	10	9	0	86	22	8
SS Oxides	0	0	12	0	14	5	4
B_4C	1	2	2	0	0	1	2

Table III. Unit 2 ex-vessel corium composition (data from chart [13]).

* Results kindly provided by David L. Luxat from Sandia National Laboratories from MELCOR code calculations.

† Stainless steel (type 304)

Species (%.wt)	Institutes			Average	Initial Inv. (Ce2)
	IBRAE	IRSN	JAEA	All institutes (Ce1)	
UO ₂	40	53	48	47	52
Zr	9	6	6	7	17
ZrO ₂	10	24	19	18	0
SS	41	17	27	28	31

3. RESULTS

3.1. Sensitivity Analysis

In addition to corium composition and MCCI progression rate (i.e. in-vessel corium/concrete ratio), three uncertain parameters were identified as possibly influencing the results: system pressure (i.e. PCV pressure), atmosphere composition (i.e. H₂O vapour and H₂ fraction in nitrogen) and the mass ratio between the corium and the atmosphere in interaction with the corium. The sensitivity is evaluated by the temperature change for which an Fe/Si ratio of 0.30, hereinafter referred to as the reference value (RV), is reached. This ratio is close to the upper value of the valid range of Fe/Si ratio for environmental CsMP (Table I).

The CIEMAT composition is used as a reference composition for the sensitivity analysis for its intermediate behaviour among the others in the following calculations.

3.1.1. System pressure

Fluctuations in system pressure do not appear to have a significant impact on the RV in the range of 1-7 bar (abs). The RV temperature varies between 1898°C and 1895°C, which is a 0.1% variation from the average absolute temperature. The pressure change is consequently considered as a negligible effect on the temperature at which the Fe/Si ratio reaches the optimal composition for CsMP generation (Figure 2).

3.1.2. Atmosphere composition

The analysis has been firstly conducted with the only consideration of H₂O and N₂ in the atmosphere. It shows that the composition of the PCV atmosphere should have a H₂O content greater than 15% for the calculation to reach the RV at a temperature of silicon-rich vapour generation. From 15% to 100% H₂O, the RV temperature differs from the average absolute temperature by only 0.6%. Then, H₂ was added up to 10% in the composition of the atmosphere and the RV temperature also differs from the average absolute temperature by less than 1%. Therefore, calculations should be performed with more than 15% H₂O, which is consistent with the accident scenario and the proportion of H₂ does not seem to affect deeply the calculations (Figure 2).

3.1.3. Mass ratio between corium and atmosphere in the control volume

The amount of atmosphere considered in our control volume is the mass of atmosphere being in equilibrium with our chemical reaction as an approximation to kinetic effects in the real case MCCI. The analysis on the mass ratio between corium and atmosphere is conducted for a ratio greater than 0.25 because either calculations do not converge for lower ratios or they provide inconsistent results in terms of temperature (Figure 2).

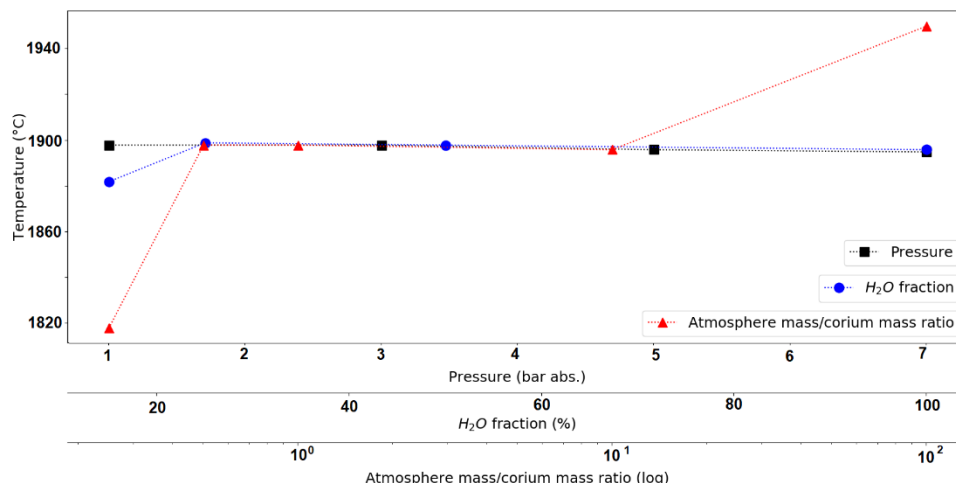


Figure 2. Sensibility analysis on three parameters considering a fixed Fe/Si ratio of 0.30.

3.1.4. Forms of Si, Fe, U and Cs in the gas phase

The assumption of using Fe/Si, U/Si and Cs/Si as indicators suggests that all forms of Si, Fe, U and Cs contribute to the CsMP generation process. To support this hypothesis, calculations on the CIEMAT composition were performed to study gas species and their proportions (species below 0.01% of the gas phase were ignored).

The major Si species in the gas phase are SiO and SiO₂. They are considered to fully participate in the generation process of the silica matrix composing the CsMP. The major Fe species in the gas phase are Fe and FeO. It has been analysed that Fe mainly exists as a divalent cation in CsMP (except on the surface layer, possibly due to weathering in the environment) as well as in its oxidation state in the FeO molecule [32]. The metallic Fe, like SiO, is likely to be oxidised in the humid atmosphere, which also leads to the formation of iron oxides. The major U species in the gas phase are UO₂ and UO₃, these oxides are likely to directly participate in the low fraction included in CsMP. Calculations imply that Cs only occurs significantly in the gas in its atomic form. The literature reports the existence of CsOH in a humid atmosphere, but as the temperature increases, CsOH tends to dissociate (around 1800°C-2200°C), especially when the atmosphere is rather reducing [33]. In conjunction with other elements not considered in these calculations, Cs can usually also form other species such as CsI, Cs_xMo_yO_z, Cs_xB_yO_z, Cs_xRu_yO_z, etc. [34]. CsI is a major concern as I is also a significant FP, but experiments showed that in steam atmosphere, only 10% of Cs would form CsI against 90% CsOH [35].

3.2. Evaluation of CsMP's Temperature of Generation without FP

As MCCI occurs, only a fraction of the corium, concrete, and gas participate in the reaction at any given time. Although these calculations are performed in thermodynamic equilibrium, by considering a fraction of each component of the system, an approximation of the kinetic effect can be achieved. The following calculations consider three cases according to the fraction of concrete in the system, representing a local corium-concrete interface condition. In the following calculations, Cs is not primarily a part of the corium composition, since the inventory fraction that might have been involved in the interaction is highly uncertain. In particular, cesium aerosols or cesium deposits on concrete surfaces may have been part of the thermodynamic system.

3.2.1. Corium-rich system

A corium rich system is simulated by a Si/Zr molar ratio of 0.10 (3.2wt% concrete for the CIEMAT composition). For each corium composition (cf. Table II & Table III), this early phase MCCI simulation

does not reach a result that could explain CsMP fabrication. In fact, the target range was reached for some compositions but at temperatures below 1000°C when Si, Fe and U releases are not significant enough to generate the particles. CsMP being mainly made of silica, this configuration may not provide enough Si for the reactions to occur.

3.2.2. Si-Zr equimolar system

This case is simulated by a Si/Zr molar ratio of 1 (25 to 50wt% concrete for all of the in-vessel compositions except IAE and KAERI).

Fe is a relevant tracer as a major element in CsMP. Moreover, Fe benefits from a consequent feedback on its thermodynamic behaviour since it has been a major concern for industrial development. Figure 3a shows that in the scope of this study, only four compositions reach the Fe/Si target range. These corium compositions are only in-vessel compositions, hence with a lower content in stainless steel (except KAERI) than ex-vessel compositions, implying that the initial stainless steel content and the oxidation rate may influence directly the Fe/Si ratio in the gas and has to be moderate to satisfy the criteria. Except for the IBRAE composition, the Fe/Si molar ratio in the gas phase appears to remain in the target range from its entry temperature to the end of the calculation range. It should be noted that the IBRAE composition is a simplified composition since it consists only of uranium oxide and non-oxidised zirconium, thus essential components participating in the chemical reactions such as stainless steel, stainless steel oxides, zirconia and boron carbide are missing. The Ci2 average in-vessel composition and the CRIEPI composition have a Zr content significantly different but show a pretty similar behaviour between 1900°C and 2600°C, meaning that the stainless steel content is more likely to be the only parameter affecting the Fe/Si ratio value, without influence of the silicon aerosols generation. At these conditions, it seems that CsMP may have been generated at a temperature above 1800-1900°C. Also, these results do not seem to show a clear upper temperature limit, but MCCI may occur at lower temperature than fuel melting temperature since concrete ablation can generally exist below 1500°C [23]. The temperature is highly dependent on the heat dissipation and production rate. These parameters are especially influenced by the debris physical configuration, the cooling efficiency (in case of cooling system at least partly operating, notwithstanding thermal radiation heat losses), the time elapsed from reactor scram, the exothermic oxidation reactions rate, etc.

Uranium is also a relevant tracer as its single source origin can be clearly identified. However, unlike Fe, U is a minor element in CsMP requiring high-precision instrumentation to be quantified or even detected in some particles. U has been identified as a segregated phase in some particles due to the capture of more minute particles in suspension in the atmosphere during CsMP growth [8]. This could influence measurements on the average concentration of U in environmental particles. The low concentration in other materials from the core such as Zr suggests that U inclusions do not originate from melt droplets or particle entrainment. It is more likely that these U particles are also a result of volatilized materials at high temperature [36]. Figure 3b shows that no composition reaches the maximum content of CsMP in U. One or several parameters in the composition yet have a significant influence on the U/Si ratio, as its value varies significantly depending on the corium composition. The initial U content does not seem to have a substantial influence since CRIEPI, as well as Ci1 and Ci2 average compositions contain almost the same amount of U but have a different behaviour. It is more likely that the environment drives these fluctuations since the corium oxidation rate appears to affect the U/Si ratio significantly: among these five corium compositions, the highest the Zr/ZrO₂ mass ratio in the composition is, the lowest the U/Si ratio in the gas phase is, with the only exception of the IAE composition which has the lowest Zr/ZrO₂ mass ratio. This exception is justified by the fact that the IAE composition is the only one containing stainless steel oxides while the others contain only metallic stainless steel. This result agrees with the U-O binary diagram suggesting that the vaporisation temperature of uranium oxides decreases with the increasing oxygen rate in the system [37]. Even if target U/Si ratio values are not reached for any composition, the CRIEPI composition approach closely the upper value around 2200°C.

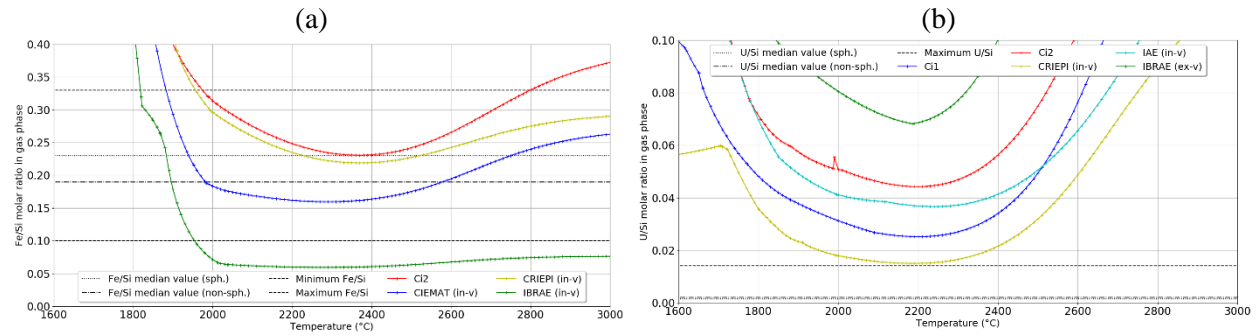


Figure 3. Temperature dependence of Fe/Si (a) and U/Si (b) molar ratio in the gas phase at Si/Zr=1 for different corium composition.

3.2.3. Concrete rich system

The concrete rich system is simulated by a Si/Zr ratio of 10, which represents more than 75wt% concrete for most compositions (66wt% for the IAE composition). It may represent a local composition near the corium-concrete interface or a more advanced phase of MCCI.

In this configuration, the different compositions seem to have more similar behaviour (explained by the dilution of corium in the concrete) with a smaller temperature variation for the same Fe/Si ratio value (Figure 4a). All of the in-vessel compositions enter the target range between 1900°C and 2100°C and most of them remain within the valid Fe/Si ratio range (Table I) up to 3000°C. Except IAE and Ci1 compositions, the median values are reached in the range of 2000-2200°C.

A higher content in the concrete also causes a reduction in the U content in the gas phase. Figure 4b shows that the temperature range for a valid U/Si ratio (Table I) value starts at a higher temperature. Most of the in-vessel compositions are close to the U/Si ratio median values around 2500-2600°C.

Calculations on ex-vessel compositions never reach any target range, this confirms expectations based on the equations (1) and (2), that a low oxidation state like in-vessel compositions favours Si rich gases and aerosols generation (Figure 3Figure 4).

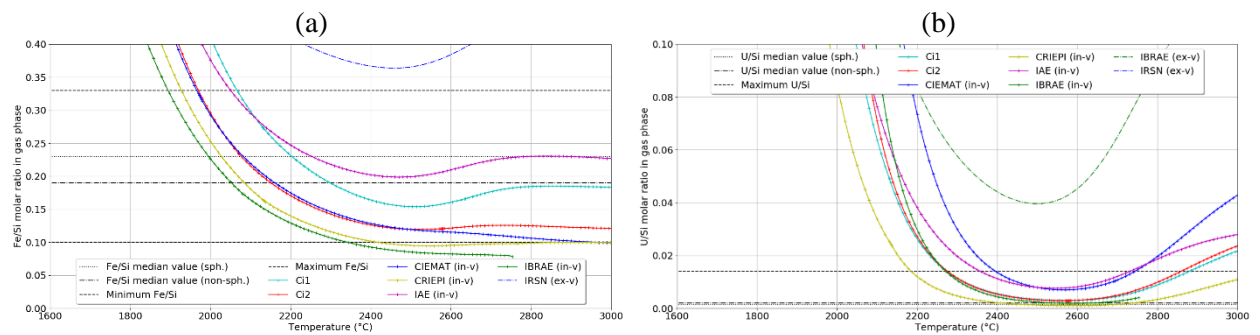


Figure 4. Temperature dependence of Fe/Si (a) and U/Si (b) molar ratio in the gas phase at Si/Zr=10 for different corium composition.

3.3. Adding Cs

The inventory of Cs in the reactor core of unit 2 (3 days after scram) was calculated to be about 1.9×10^2 kg (all Cs isotopes included), which corresponds to 2.1×10^{-3} % of the total mass of U in the core [25]. Considering the BSAF conclusions on unit 2, it was estimated for most of the institutes that the mass fraction

of the total Cs inventory vaporised from fuel (or fuel debris) does not exceed 3% in the dry well and 10% in the water of the suppression chamber by gas sparging [38].

For further calculations, the CIEMAT in-vessel composition was chosen as the reference composition as a compromise for its intermediate behaviour in Fe/Si analysis among all other satisfactory compositions. The true content of Cs participating in the generation process of CsMP is hardly definable, in particular since Cs may have been deposited on the concrete prior to corium relocation or Cs may have participated in other chemical reactions. Thus, two hypothetical cases are considered in Figure 5: 100% (in case of local high concentration) and 1% of the total Cs inventory of the reactor core (3 days after scram). Both of these cases are extreme values of Cs content; the real situation is supposedly between these two cases. These calculations suggest that the temperature should be between 1650°C and 2300°C for the vapor to have a suitable composition in Cs (Figure 5). However, it seems that the proportion of Cs that has been involved in the reaction could be significantly influenced by a few hundreds of degrees of the corium melt temperature.

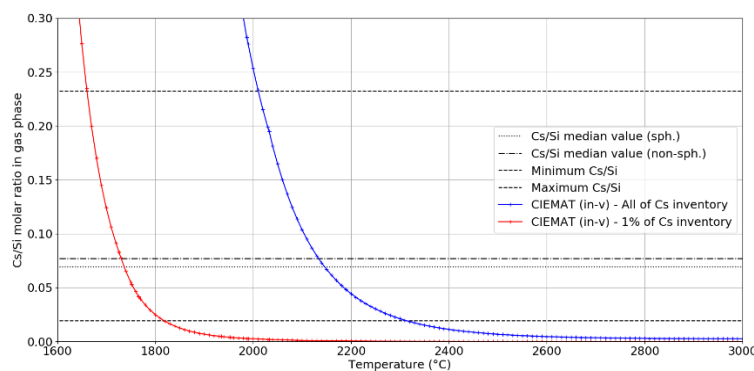


Figure 5. Temperature dependence of Cs/Si molar ratio in the gas phase at Si/Zr=1 for CIEMAT composition.

4. DISCUSSION

It should be noted that because temperature is a kinetic factor and all of these calculations were done at local thermodynamic equilibrium, they should give an accurate estimate. High temperatures are typically in favor of thermodynamic equilibrium.

In the case of an equimolar Si-Zr composition, the gas phase seems to be too rich in U species and neither composition reaches the target range. Corium heterogeneity could cause a Zircaloy-rich fraction and that is impoverished in uranium oxide to be at the origin of CsMP generation according to the chemical reactions between Zr and SiO₂. Thus, U concentration would be significantly lower in the vapours. This assumption is supported by the CRIEPI composition calculations (highest Zr/UO₂ ratio) showing the lowest U/Si ratio.

Temperatures with a U/Si ratio value in the target range (Figure 4b) match with upper temperatures for the Fe/Si ratio (Figure 3a and Figure 4a). Over several decades, numerous MCCI experiments have been performed to study interactions and temperatures of interactions. In the CCI-2 test from the Melt Attack and Coolability Experiments (MACE) program of the Argonne National Laboratories, the corium was first melted by a thermite reaction reaching 2000°C and interacting with a limestone/common sand concrete. The decay heat was simulated by direct Joule effect heating. Before water addition began, the melt temperature had decreased from approximately 1900°C at the start of the experiment to 1540°C after 300 minutes [39]. The VBU-7 test was carried out in the VULCANO facility as part of a collaboration between CEA and VTT to study corium interaction with ferro-siliceous concrete (composition very similar to 1F siliceous concrete). The corium was melted in a plasma arc furnace and the decay heat was brought by induction heating. The melt temperature in this test started out at around 2250 °C and decreased to 1550 °C after 80 minutes of

interaction [40]. An early phase MCCI is thought to have a melt temperature close to 2500°C due to the high decay heat from FP and the exothermic oxidation reactions. At the interface, the observed experimental temperature is usually lower than the suggested temperature value from Figure 4b. However, Zr oxidation that is likely to be involved in CsMP generation could locally generate a high enough temperature due to the exothermicity of the reaction between Zr and SiO₂. Then, gas generation could create sufficient convection in the melt pool to continuously bring Zr to the interface and maintain the generation process going until the oxidation rate of Zr and the concrete fraction in the melt are too high to keep the temperature sufficiently high and maintain the reaction between silica and Zr. MOCKA testing at KIT has also shown local metallic Zr and Fe residues, showing that Zr oxidation is not complete after several hours of bulk MCCI reactions [41]. Calculations performed at the thermodynamic equilibrium cannot replicate this specific observation.

Calculations also show that the stainless steel content directly affects the Fe/Si ratio. Two reasons for a low content of stainless steel in corium have been identified. The low amount of debris could be justified by a limited ablation of the internal structures, resulting in a low amount of stainless steel in the melt; or, the melt could undergo heterogeneities creating a region depleted in stainless steel and rich in Zr in favour of this behaviour. Fe content of the melt could also be increased by the dissolution of the steel from the reinforced concrete of the pedestal as observed in MOCKA experiments [41].

Calculations on aluminum were also performed but do not appear in the results as the Al/Si molar ratio was at best 10 times below the literature median values. This suggests that the modelling of the interactions of Al with the other species of the corium may suffer from an inaccurate modelling, since experiments showed that Al seems quite volatile [20].

As reported by Miura et al. [42], type-A CsMP are very likely to result from condensation of SiO vapours, especially due to their spherical shape. However, the authors conclude that the silicon of type-A CsMP comes from the eluting of the suppression chamber paint (Si < 5 wt%). Calculations reported in this present work show that a rather Si rich system would be more suitable for CsMP mass production along with a corresponding chemical composition. This statement goes in the same direction of an IRID report which asserts that the SiO₂/K₂O ratio from the paint is significantly different from the average composition ratio of CsMP, concluding that the paint could not be the only source of silicon for CsMP generation [43].

5. CONCLUSION

Equilibrium vapour compositions and Fe/Si, U/Si and Cs/Si vapour ratios during a simulated MCCI test were calculated and compared with analyses of spherical condensation particles from the simulation and also with actual type-A CsMP compositions. These preliminary experiments in VITI have indeed confirmed the possible synthesis of CsMP simulants by direct vaporisation mechanisms during the MCCI processes [20], although other multistage mechanisms such as mixing and coagulation of aerosols are also highly likely. These initial tests show that MCCI is likely to be responsible for the generation of CsMP. If the chemical composition of CsMP can be considered as an indicator of the atmosphere at the time of their formation, the corium composition that led to their generation may more closely correspond to an in-vessel corium with a low oxidation state. The calculations also suggest that the temperature was around 2000-2200°C, higher than the interface temperature of an MCCI that probably falls below 2000°C after the initial stages, possibly in a heavy metal (fuel debris) zone, that is rich in zirconium and relatively poor in stainless steel at the interface with concrete.

This paper is also preliminary work for a set of trials to be carried out at the experimental facility VITI of the PLINIUS platform at the CEA Cadarache [44]. These calculations contribute to extend the set estimated experimental parameters for generating CsMP by MCCI vapourisation.

ACKNOWLEDGMENTS

We acknowledge the helpful contribution of David L. Luxat from the Sandia National Laboratories for kindly providing us results calculated on the MELCOR code about the atmosphere inside the unit 2 PCV.

DECLARATION OF COMPETING INTERESTS

The authors declare that they have no known competing financial interests or personal relationships that could have appeared to influence the work reported in this paper.

REFERENCES

- [1] IAEA, Ed., *The Fukushima Daiichi accident*. Vienna: International Atomic Energy Agency, 2015.
- [2] IAEA, 'Live Chart of Nuclides'. <https://www-nds.iaea.org/> (accessed Feb. 08, 2023).
- [3] Y. Pontillon, G. Ducros, and P. P. Malgouyres, 'Behaviour of fission products under severe PWR accident conditions VERCORS experimental programme—Part 1: General description of the programme', *Nuclear Engineering and Design*, vol. 240, no. 7, pp. 1843–1852, Jul. 2010, doi: 10.1016/j.nucengdes.2009.06.028.
- [4] A. Stohl *et al.*, 'Xenon-133 and caesium-137 releases into the atmosphere from the Fukushima Dai-ichi nuclear power plant: determination of the source term, atmospheric dispersion, and deposition', *Atmospheric Chemistry and Physics*, vol. 12, no. 5, pp. 2313–2343, Mar. 2012, doi: 10.5194/acp-12-2313-2012.
- [5] K. Adachi, M. Kajino, Y. Zaizen, and Y. Igarashi, 'Emission of spherical cesium-bearing particles from an early stage of the Fukushima nuclear accident', *Sci Rep*, vol. 3, no. 1, p. 2554, Dec. 2013, doi: 10.1038/srep02554.
- [6] Y. Igarashi *et al.*, 'A review of Cs-bearing microparticles in the environment emitted by the Fukushima Dai-ichi Nuclear Power Plant accident', *Journal of Environmental Radioactivity*, vol. 205–206, pp. 101–118, Sep. 2019, doi: 10.1016/j.jenvrad.2019.04.011.
- [7] H. Hagiwara, H. Funaki, N. Shiribiki, M. Kanno, and Y. Sanada, 'Characterization of radiocesium-bearing microparticles with different morphologies in soil around the Fukushima Daiichi nuclear power plant', *Journal of Radioanalytical and Nuclear Chemistry*, Oct. 2021, doi: 10.1007/s10967-021-08061-8.
- [8] E. Kurihara *et al.*, 'Particulate plutonium released from the Fukushima Daiichi meltdowns', *Science of The Total Environment*, vol. 743, p. 140539, Nov. 2020, doi: 10.1016/j.scitotenv.2020.140539.
- [9] T. Ohnuki, Y. Satou, and S. Utsunomiya, 'Formation of radioactive cesium microparticles originating from the Fukushima Daiichi Nuclear Power Plant accident: characteristics and perspectives', *Journal of Nuclear Science and Technology*, vol. 56, no. 9–10, pp. 790–800, Oct. 2019, doi: 10.1080/00223131.2019.1595767.
- [10] T. Okumura, N. Yamaguchi, T. Dohi, K. Iijima, and T. Kogure, 'Dissolution behaviour of radiocaesium-bearing microparticles released from the Fukushima nuclear plant', *Sci Rep*, vol. 9, no. 1, p. 3520, Dec. 2019, doi: 10.1038/s41598-019-40423-x.
- [11] M. Suetake *et al.*, 'Dissolution of radioactive, cesium-rich microparticles released from the Fukushima Daiichi Nuclear Power Plant in simulated lung fluid, pure-water, and seawater', *Chemosphere*, vol. 233, pp. 633–644, Oct. 2019, doi: 10.1016/j.chemosphere.2019.05.248.
- [12] R. Ikehara *et al.*, 'Abundance and distribution of radioactive cesium-rich microparticles released from the Fukushima Daiichi Nuclear Power Plant into the environment', *Chemosphere*, vol. 241, p. 125019, Feb. 2020, doi: 10.1016/j.chemosphere.2019.125019.

- [13] M. Pellegrini *et al.*, ‘Main Findings, Remaining Uncertainties and Lessons Learned from the OECD/NEA BSAF Project’, *Nuclear Technology*, pp. 1–15, Apr. 2020, doi: 10.1080/00295450.2020.1724731.
- [14] H. L. Lukas, S. G. Fries, and B. Sundman, *Computational thermodynamics: the CALPHAD method*. Cambridge ; New York: Cambridge University Press, 2007.
- [15] C. Guéneau *et al.*, ‘TAF-ID: An international thermodynamic database for nuclear fuels applications’, *Calphad*, vol. 72, p. 102212, Mar. 2021, doi: 10.1016/j.calphad.2020.102212.
- [16] L. Zheng, B. Yan, B. Peng, H. Li, Z. Jiang, and S. Ueda, ‘A proposed formation mechanism of the Type-A radiocaesium-bearing microparticles released from Units 2/3 during the Fukushima Daiichi Nuclear Power Plant accident’, *Journal of Nuclear Materials*, vol. 563, p. 153623, May 2022, doi: 10.1016/j.jnucmat.2022.153623.
- [17] M. Rizaal, K. Nakajima, T. Saito, M. Osaka, and K. Okamoto, ‘Investigation of high-temperature chemical interaction of calcium silicate insulation and cesium hydroxide’, *Journal of Nuclear Science and Technology*, vol. 57, no. 9, pp. 1062–1073, Sep. 2020, doi: 10.1080/00223131.2020.1755733.
- [18] A. Hidaka, ‘Identification of Carbon in Glassy Cesium-Bearing Microparticles Using Electron Microscopy and Formation Mechanisms of the Microparticles’, *Nuclear Technology*, pp. 1–17, Aug. 2021, doi: 10.1080/00295450.2021.1929767.
- [19] N. Fujita, K. Ninomiya, Z. Zhang, A. Shinohara, and T. Yoshimura, ‘Production simulation experiments of the insoluble Cs-concentrated particles released by the FDNPP accident and their imaging on a filter’, *Proceedings of the 18th Workshop on Environmental Radioactivity*, 2017.
- [20] H. Laffolley, C. Journeau, J. Delacroix, B. Grambow, and C. Suteau, ‘Synthesis of Fukushima Daiichi Cs-bearing microparticles through molten core-concrete interaction in nitrogen atmosphere’, *Nuclear Materials and Energy*, vol. 33, p. 101253, Oct. 2022, doi: 10.1016/j.nme.2022.101253.
- [21] J. K. Fink, D. H. Thompson, B. W. Spencer, and B. R. Sehgal, ‘Aerosols released during large-scale integral MCCI tests in the ACE Program’, in *Report Number: ANL/CP-74552; CONF-9204105-5*, Research Org.: Argonne National Lab., IL (United States), Jan. 1992. [Online]. Available: <https://www.osti.gov/biblio/5710788>
- [22] D. A. Powers, J. E. Brockmann, and A. W. Shiver, ‘VANESA: a mechanistic model of radionuclide release and aerosol generation during core debris interactions with concrete’, NUREG/CR-4308, SAND-85-1370, 5150148, Jul. 1986. doi: 10.2172/5150148.
- [23] OECD/NEA, ‘State-of-the-Art Report on Molten Corium Concrete Interaction and Ex-Vessel Molten Core Coolability’, no. NEA/CSNI/R(2016)15, p. 365, 2017.
- [24] H. Alsmeyer *et al.*, ‘Molten corium/concrete interaction and corium coolability: a state of the art report’, *EUR(Luxembourg)*, 1995.
- [25] K. Nishihara, H. Iwamoto, and K. Suyama, ‘Estimation of fuel compositions in Fukushima-Daiichi nuclear power plant’, Japan, 2012. [Online]. Available: http://inis.iaea.org/search/search.aspx?orig_q=RN:44087069
- [26] TEPCO, ‘Analyses of samples related to inside survey of primary containment vessel of Unit 1-3, FDNPP.’, 2018. [Online]. Available: http://irid.or.jp/wpcontent/uploads/2018/07/20180726_02.pdf
- [27] T. Kogure *et al.*, ‘Constituent elements and their distribution in the radioactive Cs-bearing silicate glass microparticles released from Fukushima nuclear plant’, *Microscopy (Tokyo)*, vol. 65, no. 5, pp. 451–459, Oct. 2016, doi: 10.1093/jmicro/dfw030.

- [28] N. Yamaguchi, M. Mitome, A.-H. Kotone, M. Asano, K. Adachi, and T. Kogure, 'Internal structure of cesium-bearing radioactive microparticles released from Fukushima nuclear power plant', *Scientific Reports*, vol. 6, no. 1, Apr. 2016, doi: 10.1038/srep20548.
- [29] M. Pellegrini *et al.*, 'Benchmark Study of the Accident at the Fukushima Daiichi Nuclear Power Plant (BSAF Project) - Phase I Summary Report', p. 53, Feb. 2016.
- [30] D. Peko, S. Basu, S. Kraft, S. Mizokami, and J. Rempe, 'Working together to enhance nuclear reactor safety', p. 7.
- [31] V. Bouyer *et al.*, 'Large scale Vulcano molten core-concrete interaction test considering Fukushima Daiichi condition', *The 9TH European Review Meeting on Severe Accident Research (ERMSAR2019)*, Prague, Czech Republic, 2019.
- [32] T. Okumura, N. Yamaguchi, H. Suga, Y. Takahashi, H. Segawa, and T. Kogure, 'Reactor environment during the Fukushima nuclear accident inferred from radiocaesium-bearing microparticles', *Sci Rep*, vol. 10, no. 1, p. 1352, Dec. 2020, doi: 10.1038/s41598-020-58464-y.
- [33] L. Devell and K. Johansson, 'Specific features of cesium chemistry and physics affecting reactor accident source term predictions', OECD/NEA and SKI, SKI Report 94:29, Aug. 1994.
- [34] M. Osaka, M. Gouëllou, and K. Nakajima, 'Cesium Chemistry in the LWR severe accident and towards the decommissioning of Fukushima Daiichi Nuclear Power Station', *Journal of Nuclear Science and Technology*, pp. 1–14, Dec. 2021, doi: 10.1080/00223131.2021.1997664.
- [35] M. F. Osborne and R. A. Lorenz, 'ORNL studies of fission product release under LWR severe accident conditions', *nuclear safety*, vol. 33, no. 3, pp. 344–365, 1992.
- [36] A. Ochiai *et al.*, 'Uranium Dioxides and Debris Fragments Released to the Environment with Cesium-Rich Microparticles from the Fukushima Daiichi Nuclear Power Plant', *Environmental Science & Technology*, vol. 52, no. 5, pp. 2586–2594, Mar. 2018, doi: 10.1021/acs.est.7b06309.
- [37] C. Guéneau *et al.*, 'Thermodynamic modelling of advanced oxide and carbide nuclear fuels: Description of the U–Pu–O–C systems', *Journal of Nuclear Materials*, vol. 419, no. 1–3, pp. 145–167, Dec. 2011, doi: 10.1016/j.jnucmat.2011.07.033.
- [38] M. Sonnenkalb *et al.*, 'Overview and outcomes of the OECD/NEA benchmark study of the accident at the Fukushima Daiichi NPS (BSAF), phase 2 – Results of severe accident analyses for unit 2', *Nuclear Engineering and Design*, vol. 369, p. 110840, Dec. 2020, doi: 10.1016/j.nucengdes.2020.110840.
- [39] M. T. Farmer, S. Lomperski, D. J. Kilsdonk, R. W. Aeschlimann, and S. Basu, 'OECD MCCI project 2-D Core Concrete Interaction (CCI) tests : CCI-2 test data report-thermalhydraulic results. Rev. 0 October 15, 2004.', OECD/MCCI-2005-TR04, 1014856, 2004. doi: 10.2172/1014856.
- [40] T. Sevón, C. Journeau, and L. Ferry, 'VULCANO VB-U7 experiment on interaction between oxidic corium and hematite-containing concrete', *Annals of Nuclear Energy*, vol. 59, pp. 224–229, Sep. 2013, doi: 10.1016/j.anucene.2013.04.016.
- [41] X. Gaus-Liu, T. Cron, D. Bottomley, and B. Fluhrer, 'MCCI ON SILICEOUS AND LCS CONCRETE WITH OXIDE AND METALLIC MELT: RE-EVALUATION OF MOCKA EXPERIMENTS', *19th International Topical Meeting on Nuclear Reactor Thermal Hydraulics (NURETH-19)*, 2022.

- [42] H. Miura *et al.*, 'Characterization of two types of cesium-bearing microparticles emitted from the Fukushima accident via multiple synchrotron radiation analyses', *Scientific Reports*, vol. 10, no. 1, Dec. 2020, doi: 10.1038/s41598-020-68318-2.
- [43] IRID, 'Decommissioning / contaminated water countermeasure project cost subsidy (advancement of comprehensive understanding of the situation inside the reactor) (Japanese translation) - International Research Institute for Nuclear decommissioning', 2018. Accessed: Jun. 23, 2020. [Online]. Available: https://irid.or.jp/_pdf/20170000_01.pdf
- [44] C. Journeau *et al.*, 'Upgrading the PLINIUS platform toward smarter prototypic-corium experimental R&D', *Nuclear Engineering and Design*, vol. 386, p. 111511, Jan. 2022, doi: 10.1016/j.nucengdes.2021.111511.